Robotica (2019) volume 37, pp. 213–232. © Cambridge University Press 2018
doi:10.1017/S0263574718000954

Operational performance analysis of spiral capsule robot in multiphase fluid

Liang Liang†,* Bai Chen‡, Yong Tang†, Yan Xu† and Yu Liu†

†*School of Mechanical and Electrical Engineering, Changsha University, Changsha 410022, China*
‡*Jiangsu Key Laboratory of Precision and Mico-Manufacturing Technology, Nanjing University of Aeronautics and Astronautics, Nanjing 210016, China*

(Accepted August 25, 2018. First published online: September 19, 2018)

SUMMARY
Minimally invasive surgery is a developing direction of modern medicine. With the successful development of controllable capsule endoscopies, capsule robots are very popular in the field of gastrointestinal medicine. At present, the study of intestinal robots is aimed at the pipeline environment of a single-phase liquid flow. But there exist food residues (i.e. solid particles) or liquid foods in the actual intestine, so intestinal fluid should be liquid–solid or liquid–liquid two-phase mixed fluid. For inner spiral capsule robots with different internal diameters and outer spiral capsule robots, using computational fluid dynamics (CFD) method, the operational performance indicators (i.e. axial thrust force, circumferential resisting moment and maximum pressure to pipeline wall) of spiral capsule robots are numerically calculated in the liquid–solid or liquid–liquid two-phase mixed fluid. By the orthogonal experimental optimization method, the optimum design of spiral capsule robots is obtained in the liquid–solid mixed fluid. The experimental verification has been also carried out. The results show that in the liquid–solid two-phase fluid, the axial thrust force and circumferential resisting moment of the spiral capsule robots decrease with the increase of the size or concentration of solid particles. In the same liquid–solid or liquid–liquid mixed fluid, the operational performance indicators of outer spiral robots are much higher than those of inner spiral robots, and the operational performance indicators of inner spiral robots with bigger internal diameters are higher than those with smaller internal diameters. Adding solid particles of high concentration in the pipeline containing liquid will reduce the drive performance of spiral capsule robots, but adding another liquid of high viscosity will improve the drive performance of spiral capsule robots.

KEYWORDS: Liquid–solid two-phase fluid, Liquid–liquid two-phase fluid, Spiral capsule robots, Computational fluid dynamics, Operational performance

1. Introduction

Robotic surgery is one of the directions of modern medical development. Among them, capsule robots are a class of important medical robots. At present, the remote control capsule endoscopy has become an actual intestinal examination robot.[1]

Intestinal capsule robots are mainly divided into two categories, one is the mobile capsule robot, and the other is the spiral capsule robot. Passive capsule endoscopy is the earliest type of mobile capsule robot that relies on the peristalsis of the intestinal tract to drive the movement of the capsule endoscope.[2–5] Then, an active mobile capsule robot emerges. The bionic capsule robots that simulate worms or earthworms have been developed.[6–8] Zhang et al.[9] developed a capsule robot that uses capsule internal forces and intestinal environmental friction. Woo[10] et al. studied an electrically

* Corresponding author. E-mail: fatliangliang@126.com
E-mail: tangyong@ccsu.edu.cn, xuyan@ccsu.edu.cn, wind_liuyu@163.com, chenbye@nuaa.edu.cn

propelled intestinal capsule robot. He et al.[11] designed an expanding–extending robotic capsule endoscope, which includes two clamp legs at the end, an intermediate retractor and a camera module. All of the above mobile capsule robots rely on the frictional force between their working surfaces and the inner wall of the intestine as the driving force regardless of the different structures. Their control is relatively easy to achieve, but there may be some damage to the inner wall of the intestine.

Since the screw thread can convert the rotational motion into a linear motion, the spiral capsule robot is a kind of precession-type capsule robot. When it rotates at a high speed in a pipeline filled with viscous liquid (the diameter of the pipeline is larger than the diameter of the robot), the liquid will generate thrust force and dynamic pressure, and the movement form of the robot is a suspension-type precession movement. Spiral capsule robots mainly include outer spiral capsule robots and inner spiral capsule robots. The outer spiral intestinal capsule robots driven by external magnetic fields have been theoretically and experimentally studied,[12–16] as shown in Fig. 1. The outer spiral capsule robot has a relatively larger thrust force, but when its diameter is larger than that of the pipeline, it will be in contact with the inner wall of the intestine, and the friction is relatively larger, which may damage the intestine. Liang et al.[17] first proposed a novel inner and outer spiral micro in-pipe robot, and then proposed an inner spiral capsule robot with smooth shells driven by external magnetic fields, as shown in Fig. 2.[18] Although the thrust force of inner spiral capsule robots is relatively smaller, based on the smooth shells, the damage to the intestine is relatively smaller.[19]

Intestinal fluid is produced by intestinal glands and epithelial cells, most of which is water, and it is a viscous liquid. In the current research literature, in the study of various types of intestinal capsule robots, intestine fluids are assumed to be single-phase fluids such as silicone oil, that is, liquids. Zhou et al.[20] found that the apparent viscosity of large intestine mucus is lower than that of small intestine mucus and gastric juice at a low shear rate. The apparent viscosity of digestive tract mucus decreases rapidly with the increase of shear rate, and it is manifested as pseudoplastic non-Newtonian fluid; when the shear rate arrives to a certain value, the apparent viscosity of the digestive tract mucus is constant, showing the characteristics of Newtonian fluid. Wang et al.[21] found that intestinal mucus can reduce the intestinal friction coefficient to 10^{-2} orders of magnitude. However, in the actual human intestines, there exist food residues (i.e. solid particles) or liquid foods. At this time, the intestinal fluid can be considered as a liquid–solid two-phase mixed fluid.

Based on dynamics equations in the multiphase mixed fluid, the computational fluid dynamics (CFD) method is used to calculate the operational performance indicators (i.e. axial thrust force, circumferential resisting moment and maximum pressure to pipeline wall) of inner spiral capsule robots with different internal diameters and outer spiral capsule robots, and the influences of the size of solid particle (i.e. particle diameter), the concentration of solid particle (i.e. the volume ratio of the solid particle in the mixed fluid) and the concentration of the second-phase liquid (i.e. the volume ratio of the second-phase liquid in the mixed fluid) on the operational performance of the robots. The optimum structure of spiral capsule robots is designed in the liquid–solid mixed fluid. The driving laws of spiral robots in the multi-phase fluid are obtained. This lay a solid theoretical foundation of spiral capsule robots to be used in the intestines (or blood vessels).

2. Structures of Spiral Capsule Robots

Figures 1 and 2 are, respectively, outer and inner spiral capsule robots in the pipeline filled with multiphase fluid. The external magnetic field drives the permanent magnets in the robots rotate in high speed, and the rotating spiral surface will generate the liquid reaction thrust. And due to the fluid dynamic effect, the spiral robots move in the pipeline in the suspended state. In contrast, an outer spiral robot has bigger drive force and more energy consumption, and an inner spiral robot has a smooth shell and less damage. Different spiral capsule robots can be chosen according to different application requirements.

3. Hydrodynamic Equations of Mixed Fluid

When the pipeline is filled with liquid–solid or liquid–liquid mixed fluid, the force of the spiral robot can be obtained by the mixed fluid flow field near the robot. It is assumed that the liquid–solid or liquid–liquid two-phase mixed fluid is the continuous continuum that two phase fluids are interspersed with each other. The continuous and momentum equations of the mixed fluid are as follows:[22]

https://doi.org/10.1017/S0263574718000954 Published online by Cambridge University Press

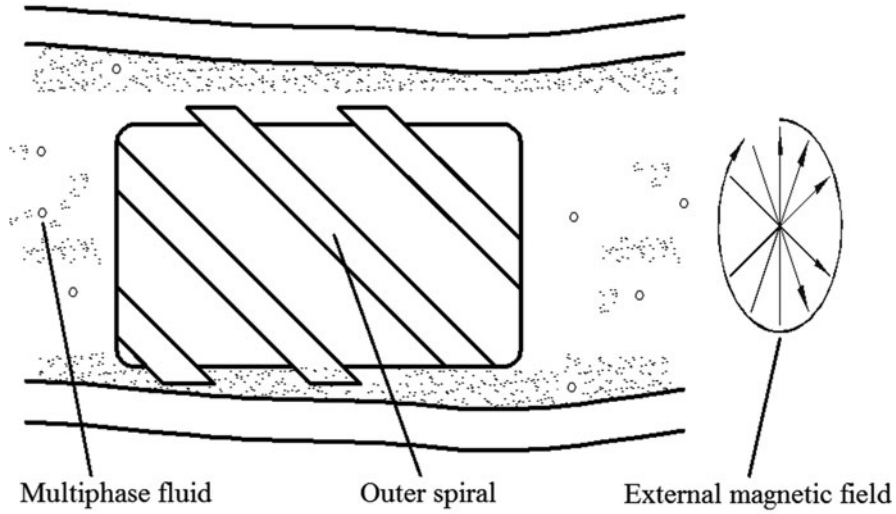

Fig. 1. An outer spiral capsule robot in multiphase fluid.

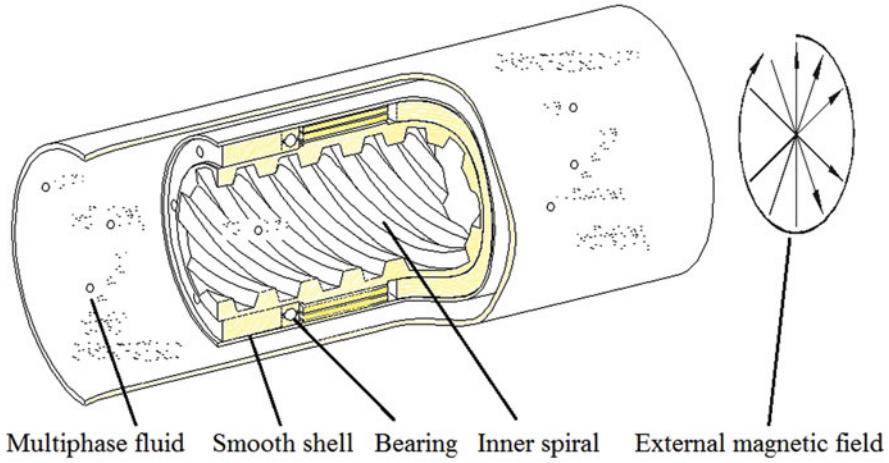

Fig. 2. An inner spiral capsule robot in multiphase fluid.

Continuous equations

$$\frac{\partial \rho}{\partial t} + \nabla \cdot (\rho \boldsymbol{v}) = 0 \tag{1}$$

Momentum equations

$$\frac{\partial}{\partial t}(\rho \boldsymbol{v}) + \nabla \cdot \left(\rho \boldsymbol{v}^2\right) = -\Delta \boldsymbol{p} + \nabla \cdot [\mu_m(\nabla \boldsymbol{v} + \nabla \boldsymbol{v}^{\boldsymbol{T}})] + \rho \boldsymbol{g} + \boldsymbol{F} + \nabla \cdot \left(\sum_{k=1}^{n} \alpha_k \rho_k \boldsymbol{v}_{\boldsymbol{k}}^{\boldsymbol{r}^2}\right) \tag{2}$$

$$\boldsymbol{v}_{\boldsymbol{k}}^{\boldsymbol{r}} = \boldsymbol{v}_{\boldsymbol{k}} - \boldsymbol{v} \tag{3}$$

where Hamiltonian differential operator $\nabla = \boldsymbol{i}\frac{\partial}{\partial x} + \boldsymbol{j}\frac{\partial}{\partial y} + \boldsymbol{k}\frac{\partial}{\partial z}$; $\boldsymbol{i}$, $\boldsymbol{j}$ and $\boldsymbol{k}$ are unit vectors in the x-, y- and z-direction, respectively; ρ is the density of mixed fluid; $\boldsymbol{v}$ is the velocity vector of mixed fluid; $\boldsymbol{p}$ is static pressure vector; μ_m is mixed viscous coefficient; $\boldsymbol{g}$ is gravity acceleration vector; $\boldsymbol{F}$ is volume force; n is phase numbers; α_k is the volume ratio of the kth phase fluid; ρ_k is the density of the kth phase fluid; and $\boldsymbol{v}_{\boldsymbol{k}}$ is the velocity vector of the kth phase fluid.

https://doi.org/10.1017/S0263574718000954 Published online by Cambridge University Press

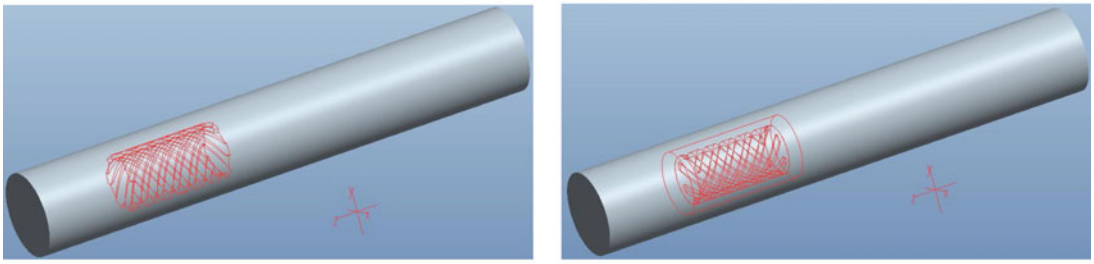

(a) (b)

Fig. 3. Geometric calculation model of spiral robots: (a) outer spiral and (b) inner spiral.

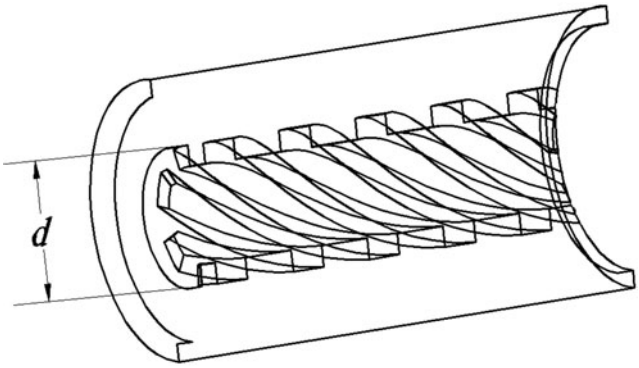

Fig. 4. Bottom diameter of the inner spiral groove of an inner spiral robot.

It is difficult to obtain the analytic solution of the above equations, and the CFD method can be used to solve the approximate solution satisfying the actual requirements. The solving steps are as follows: modeling three-dimensional robot system; meshing robot system and setting boundary conditions; and setting solution parameters and solving. The correctness and validity of the above numerical calculation method have been verified in the literature.[18]

The difference between the approximate solutions using the CFD method and the exact solutions of the above theoretical equations is influenced by many factors, including the accuracy of the established geometric model, the size and quality of the meshes, the setting of boundary conditions and the selection of the solution parameters (the discretized schemes, the calculation method of the flow field, the turbulence model, calculation model of multiphase flow, convergence accuracies, etc.). The difference between the numerical results and the experimental results also depends on the mixing state of the multiphase fluid, the material of the pipeline and so on.

4. Numerical Calculation Model and Method

4.1. Calculation model of robot system

The geometric calculation model of the robot system is shown in Fig. 3. It is assumed that the pipeline diameter is 12 mm and its length is 75 mm, and central axis of the robot and that of pipeline coincides. It is defined that the bottom diameter of the inner spiral groove is indicated by d, as shown in Fig. 4. The spiral capsule robots all have rectangular spiral grooves, and the parameters are listed in Table I.

4.2. Meshing of robot system

Meshing refers to the meshing of the fluid zones in the working pipeline. The outer spiral robot system comprises two fluid zones, and the inner spiral robot system comprises three fluid zones. The fluid zones of the outer spiral robot include the adjacent zone (Zone b) of outer spiral surfaces and the remaining zone (Zone c), as shown in the blue zones of Fig. 5. The fluid zones of the inner spiral robot include the adjacent zone (Zone a) of inner spiral surfaces, the adjacent zone (Zone b) of smooth

https://doi.org/10.1017/S0263574718000954 Published online by Cambridge University Press

Table I. Parameters of spiral capsule robots.

Parameters	Outer spiral capsule robot	Inner spiral capsule robot
Outer diameter of the robot (mm)	8	8
Robot axial length (mm)	15	15
Number of threads	6	6
Thread lead (mm)	15	15
Width of the groove top (mm)	1	1.5
Width of the groove bottom (mm)	1.5	1
Groove depth (mm)	0.6	0.6
Bottom diameter of inner spiral groove (mm)	–	4, 7

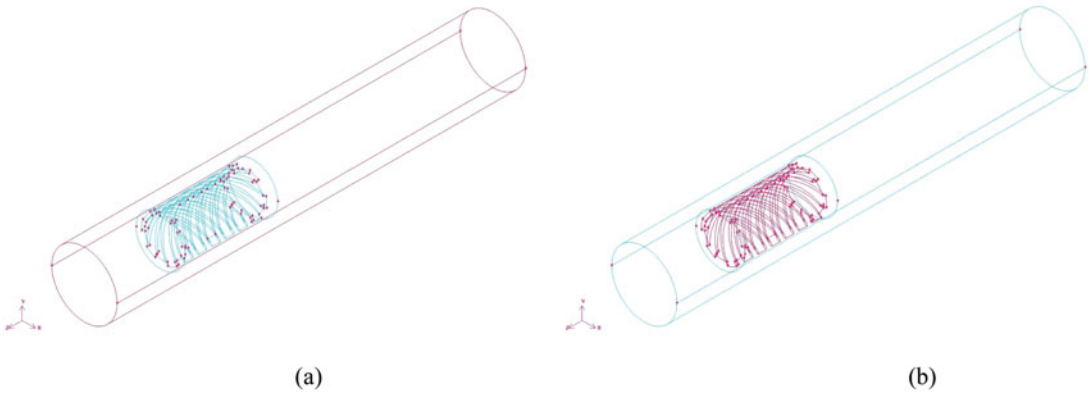

Fig. 5. Fluid zones of the outer spiral capsule robot system: (a) zone adjacent to the outer spiral surfaces and (b) remaining zone.

outer surfaces and the remaining zone (Zone c), as shown in the blue zones of Fig. 6. For the size of adjacent zone (Zone b) of outer spiral surfaces of the outer or inner spiral capsule robot, the axial thickness around both ends of the robot is 1 mm, and the circumferential thickness around the robot is 0.5 mm. The sizes of other fluid zones can be calculated accordingly. Taking into account the geometric shapes of all fluid zones, the dense meshes are used at the fluid zones adjacent to spiral surfaces. The divided meshes of the spiral capsule robot system are showed in Fig. 7. The mesh quality is checked, and if the maximum cell skewness is smaller than 0.82, the mesh meets the computing requirements.

4.3. Setting of solving parameters and comparison of influencing factors

In the numerical calculation, the mesh type and number, the robot operating parameters, the nature of the working pipeline, the solid-phase parameters, two kinds of liquid-phase parameters and the calculation convergence accuracies are shown in Table II. In the liquid–liquid two-phase fluid, the density of the added liquid phase is not changeable and the dynamic viscosity becomes higher. In the liquid–solid two-phase fluid, the added solid-phase particle is similar to sand.

In order to obtain the reasonable calculation results, the standard k–ϵ model is chosen in the fluid turbulent flow, and the fluid flow near the wall is treated with the standard wall function. The hybrid model is used in the multiphase flow. The fluid gravity is considered, and its direction is negative y-axial direction. To solve the pressure and velocity coupling equations of the fluid flow field, the standard SIMPLE algorithm is used. The pressure is discretized by the PRESTO! scheme, the momentum is discretized by the first-order upwind scheme and the turbulent kinetic energy (k) and dissipation rate (ϵ) are discretized by the second-order upwind scheme. In order to simulate the movement of the fluids near the spiral surfaces, the multi-reference frame is used. The rotational speed of the rotating spiral wall surfaces is equal to the speed of the adjacent fluid. The steady calculation is used. The pipeline inlet is set close to one end of the robot, and the pipeline outlet is set away from one end of

https://doi.org/10.1017/S0263574718000954 Published online by Cambridge University Press

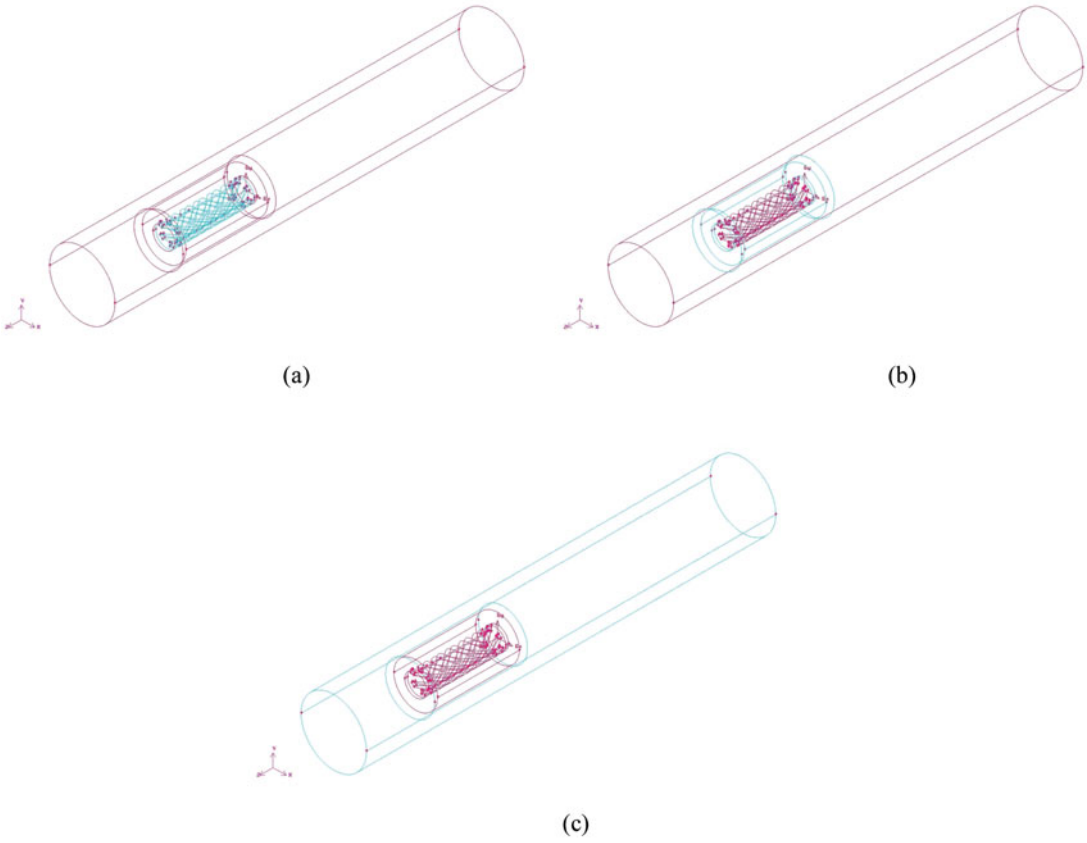

Fig. 6. Fluid zones of the inner spiral capsule robot system: (a) zone adjacent to the inner spiral surfaces, (b) zone adjacent to the smooth outer surfaces and (c) remaining zone.

Table II. Mesh parameters and solving parameter setting values.

Parameters	Outer spiral capsule robot	Inner spiral capsule robot ($d = 4$ mm)	Inner spiral capsule robot ($d = 7$ mm)
Mesh type	Tetrahedron	Tetrahedron	Tetrahedron
Mesh number	88,816	102,335	133,464
Outer surfaces of the robot (rpm)	600	0	0
Inner surfaces of the robot (rpm)	–	600	600
Moving speed of the robot (m/s)	0		
Moving speed of the fluid (m/s)	0		
Operating state of the robot	Suspension (central axis of the robot and that of pipeline coincide)		
Nature of working pipeline	Rigidity		
Density of the liquid phase (kg/m^3)	1000		
Dynamic viscosity of the liquid phase (Pa·s)	1		
Density of the added second-phase liquid (kg/m^3)	1000		
Dynamic viscosity of the added second-phase liquid (Pa·s)	10		
Density of the added solid-phase particle (kg/m^3)	1200		
Dynamic viscosity of the added solid-phase particle (Pa·s)	10^{-4}		
Diameter of the solid phase (mm)	0.1∼0.9		
Concentration of the solid phase	0.1∼0.9		
Convergence accuracies (continuity, x-, y-, z-axial directional velocity, k and ϵ)	0.001		

https://doi.org/10.1017/S0263574718000954 Published online by Cambridge University Press

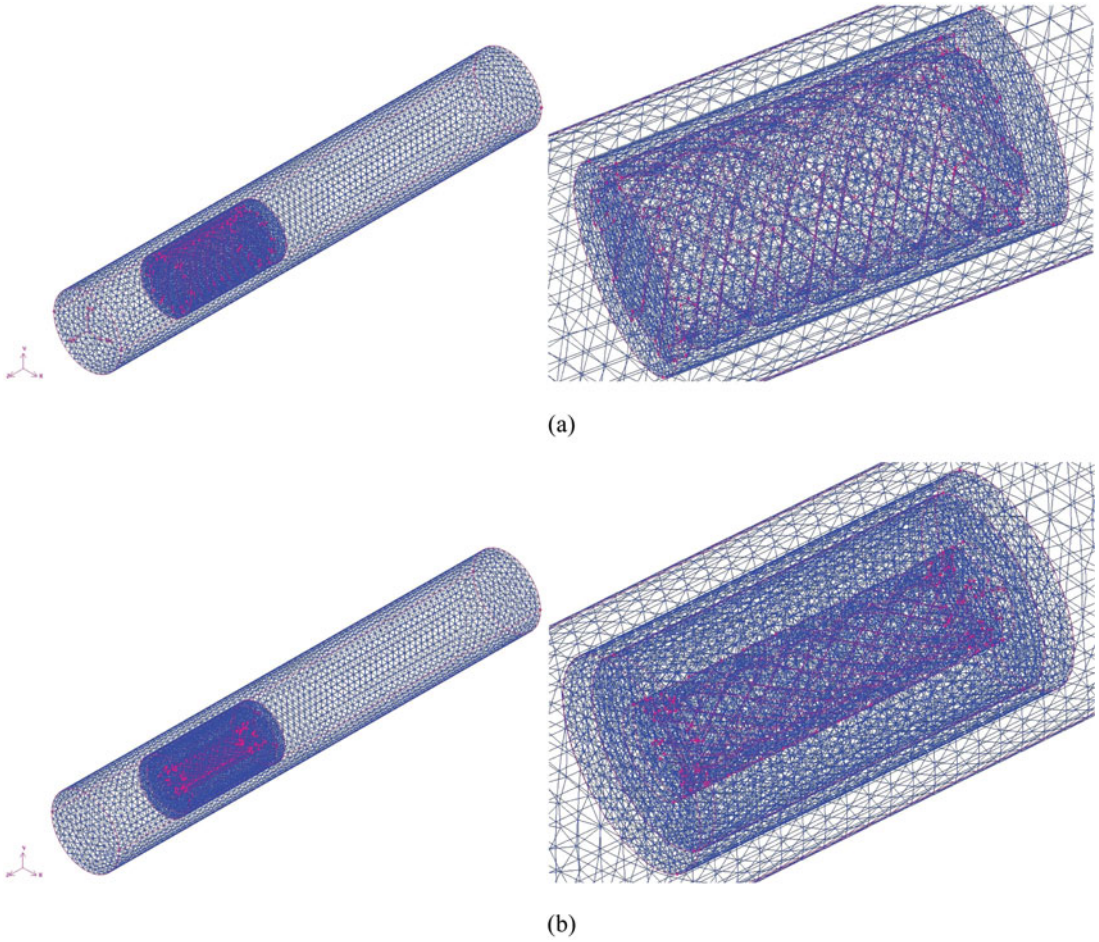

Fig. 7. Divided meshes of the spiral capsule robot system: (a) whole and enlarged views of the outer spiral capsule robot and (b) whole and enlarged views of the inner spiral capsule robot.

the robot. The boundary conditions are the pressure inlet and the pressure outlet, and the initial values are all zeros at all zones.

As noted previously, the CDF method used in this paper is to numerically solve the mass and momentum equations of the mixed fluid near the spiral capsule robots to obtain the force of the robots. The difference between the approximate numerical results and the exact theoretical results or actual experimental results is related to various factors, such as mesh sizes, mesh quality, discretized schemes of variables, pipeline nature, the homogeneous degree of two phase fluids, calculation model of multiphase flow, convergence accuracies and so on.

Assuming that the two-phase fluids are homogeneously mixed and the pipeline is rigid, the effects of different size meshes and discretized schemes on the numerical results are calculated and analyzed. Table III shows the mesh sizes and discretized schemes of some variables of two kinds of spiral capsule robots in three cases. Table IV shows their performance indicators in the three cases.

According to the two tables, the mesh size has a little influence on the numerical results, while the discretized scheme has a little influence. When the mesh size is decreased, the performance indicators of the inner spiral capsule robot are slightly decreased, but those of the outer spiral capsule robot are slightly increased.

Therefore, the most important factor in the numerical calculation is the mesh size. Under meeting the requirements of the mesh quality, the appropriate mesh size should be selected to obtain the optimal calculation time and calculation results. The parameter values of No. 2 and No. 5 are adopted in the subsequent calculation.

https://doi.org/10.1017/S0263574718000954 Published online by Cambridge University Press

Table III. Different mesh sizes and discretized schemes of some variables in three cases.

No.	Meshed interval sizes			Discretized schemes			
	Zone a	Zone b	Zone c	Pressure	Momentum	Turbulent kinetic energy	Dissipation rate
				Inner spiral capsule robot ($d = 4$ mm)			
1	0.35	0.45	0.9	PRESTO!	First-order upwind	Second-order upwind	Second-order upwind
2	**0.4**	**0.5**	**1**	**PRESTO!**	**First-order upwind**	**Second-order upwind**	**Second-order upwind**
3	0.4	0.5	1	PRESTO!	First-order upwind	First-order upwind	First-order upwind
				Outer spiral capsule robot			
4	–	0.45	0.9	PRESTO!	First-order upwind	Second-order upwind	Second-order upwind
5	–	**0.5**	**1**	**PRESTO!**	**First-order upwind**	**Second-order upwind**	**Second-order upwind**
6	–	0.5	1	PRESTO!	First-order upwind	First-order upwind	First-order upwind

Table IV. Performance indicators of spiral capsule robots in three cases.

No.	Robot type	Axial thrust force (mN)	Circumferential resisting moment (mN·m)	Maximum pressure to pipeline wall (Pa)
1	Inner spiral capsule robot ($d = 4$ mm)	0.0369	0.00207	0.82
2		**0.0559**	**0.00213**	**0.84**
3		0.0560	0.00213	0.83
4	Outer spiral capsule robot	2.794	0.381	45.48
5		**2.643**	**0.375**	**24.78**
6		2.625	0.373	24.45

5. Operational Performances of Spiral Capsule Robots in Multiphase Fluid

5.1. Liquid–solid two-phase fluid environment

The operational performance indicators of spiral capsule robots mainly include axial thrust force of the robot, circumferential resisting moment of the robot and maximum pressure to pipeline wall. In order to study the effect of solid particles on the operational performance of spiral capsule robots, it is assumed that the added solid-phase particles are dispersed homogeneously in the liquid phase, the particle diameter changes from 0.1 mm to 0.9 mm and the particle concentration changes from 0.1 to 0.9.

5.1.1. Effect of the sizes of solid-phase particles. Figures 8 to 10 are, respectively, the variation curves of the robotic performance indicators with the sizes of solid-phase particles in the single-phase liquid and the liquid–solid two-phase fluid when the particle concentration is 0.1. In the figure, the particle diameter is 0 to represent the single-phase liquid. In the liquid–solid two-phase fluid, when the particle diameter is increased, the axial thrust force and circumferential resisting moment of the spiral capsule robots decrease slowly, while the maximum pressure to pipeline wall decreases or increases, and the value changes little. The performance indicators of the outer spiral robot are much higher than those of the inner spiral robot, and the performance indicators of inner spiral robots with bigger internal diameters are higher than those with smaller internal diameters. For inner spiral capsule robots with the bottom diameters of the inner spiral grooves of 4 mm and 7 mm, when the bottom diameter (d) is increased, the area of the inner spiral surface of the robot will be increased. As a result, the fluid area in contact with the spiral surface of the robot is increased, and the operating performance indicators of the robot will be increased. At the same time, the axial thrust force of spiral capsule robots in the liquid–solid two-phase fluid is lower than that in the single-phase liquid, which indicates that the addition of solid particles in the pipeline containing liquid will reduce the drive performance of the spiral capsule robot.

https://doi.org/10.1017/S0263574718000954 Published online by Cambridge University Press

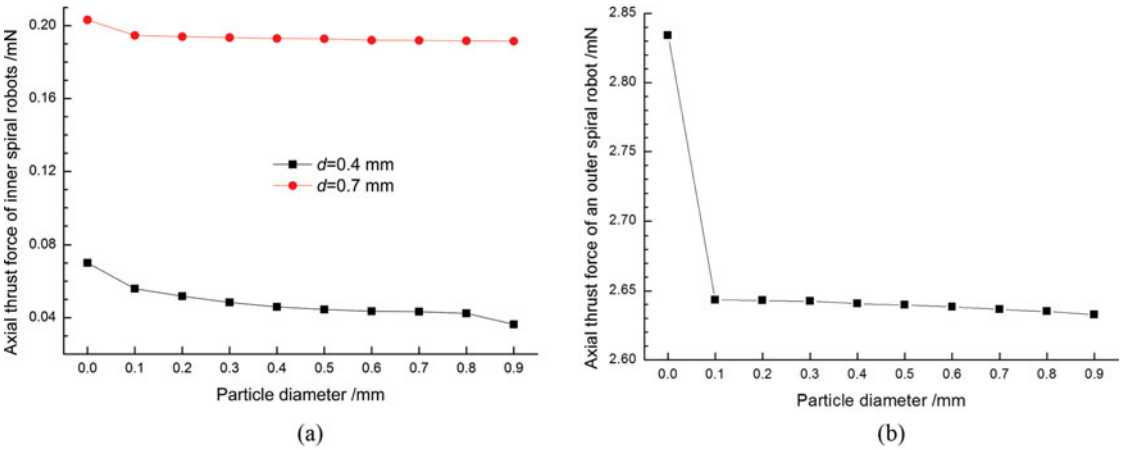

Fig. 8. Relationship between axial thrust force of the robot and sizes of solid-phase particles: (a) inner spiral robot and (b) outer spiral robot.

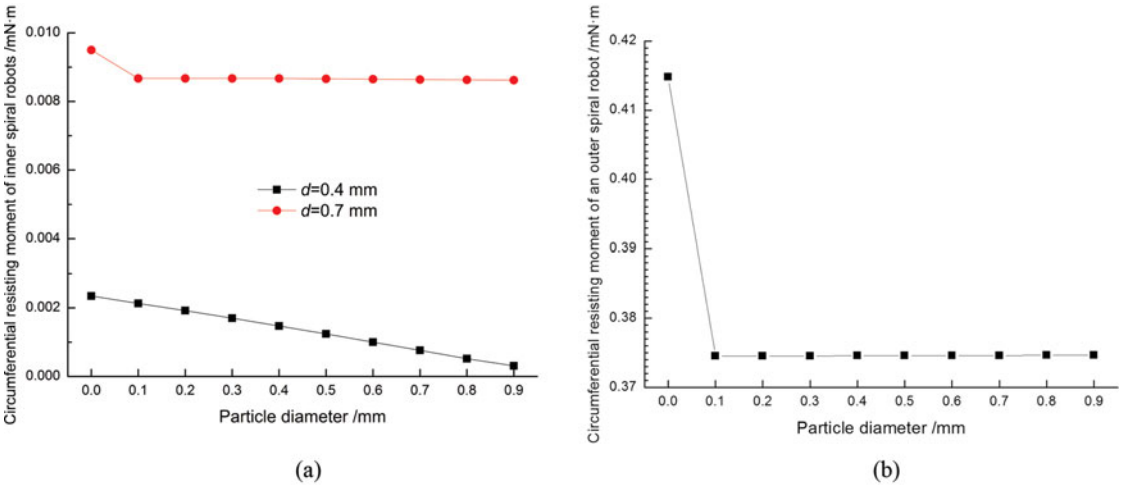

Fig. 9. Relationship between circumferential resisting moment of the robot and sizes of solid-phase particles: (a) inner spiral robot and (b) outer spiral robot.

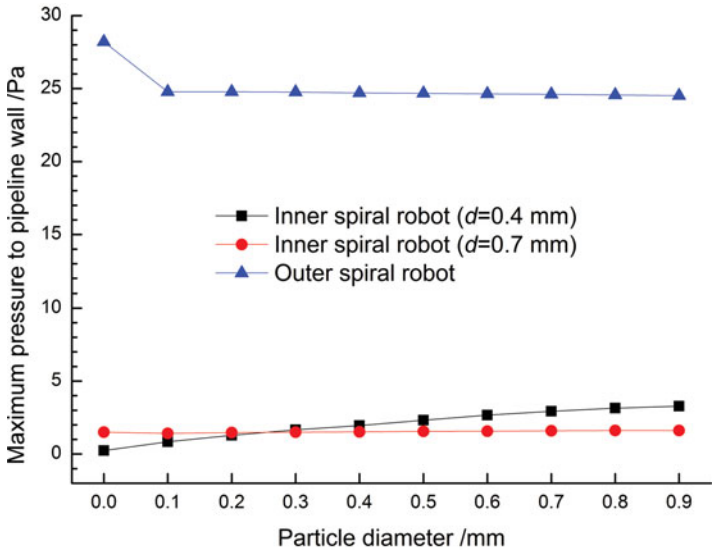

Fig. 10. Relationship between maximum pressure to pipeline wall and sizes of solid-phase particles.

https://doi.org/10.1017/S0263574718000954 Published online by Cambridge University Press

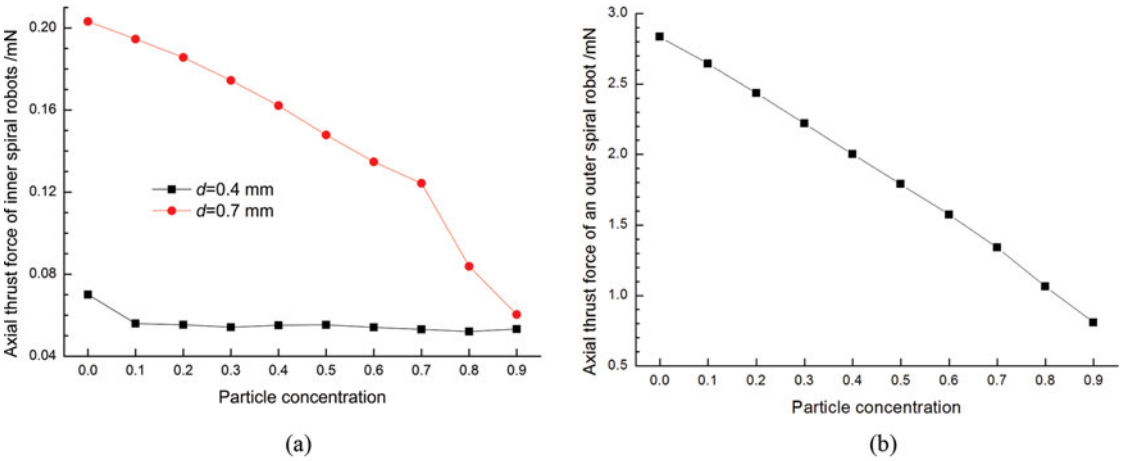

Fig. 11. Relationship between axial thrust force of the robot and concentrations of solid-phase particles: (a) inner spiral robot and (b) outer spiral robot.

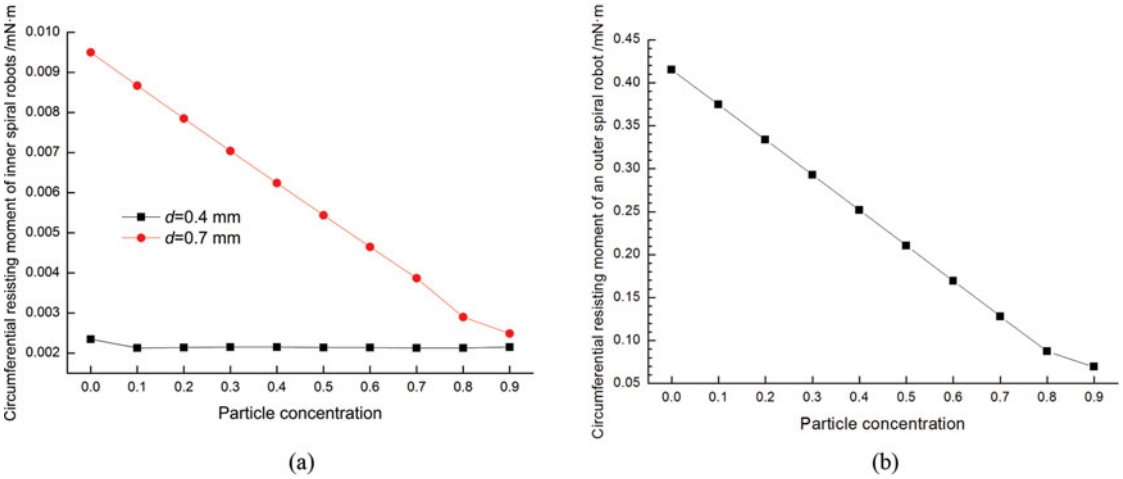

Fig. 12. Relationship between circumferential resisting moment of the robot and concentrations of solid-phase particles: (a) inner spiral robot and (b) outer spiral robot.

5.1.2. Effect of the concentrations of solid-phase particles. Figures 11 to 13 are, respectively, the variation curves of the robotic performance indicators with the concentrations of solid-phase particles in the single-phase liquid and the liquid–solid two-phase fluid when the particle diameter is 0.1 mm. In the figure, the particle concentration is 0 to represent the single-phase liquid. In the liquid–solid two-phase fluid, when the particle concentration is increased, the axial thrust force and circumferential resisting moment of the spiral capsule robots decrease, while the maximum pressure to pipeline wall decreases or increases. This shows that in the single-phase liquid, when the concentration of added solid particles is increased, the operational performance of the spiral robot will be reduced. Similarly, in the liquid–solid mixed fluid with different concentrations of solid particles, the performance indicators of the outer spiral robot are much higher than those of the inner spiral robot, and the performance indicators of inner spiral robots with bigger internal diameters are higher than those with smaller internal diameters. In Fig. 11(a), when the concentration of solid-phase particles is changed from 0.7 to 0.9, the axial thrust force of the inner spiral robot ($d = 7$ mm) is suddenly decreased. This is due to the increase of the solid particle concentration, and the degree of turbulence of fluid near the inner surface of the robot with larger bottom diameter of inner spiral grooves is strengthened, which greatly reduces the thrust force of the fluid on the inner spiral surfaces of the robot.

https://doi.org/10.1017/S0263574718000954 Published online by Cambridge University Press

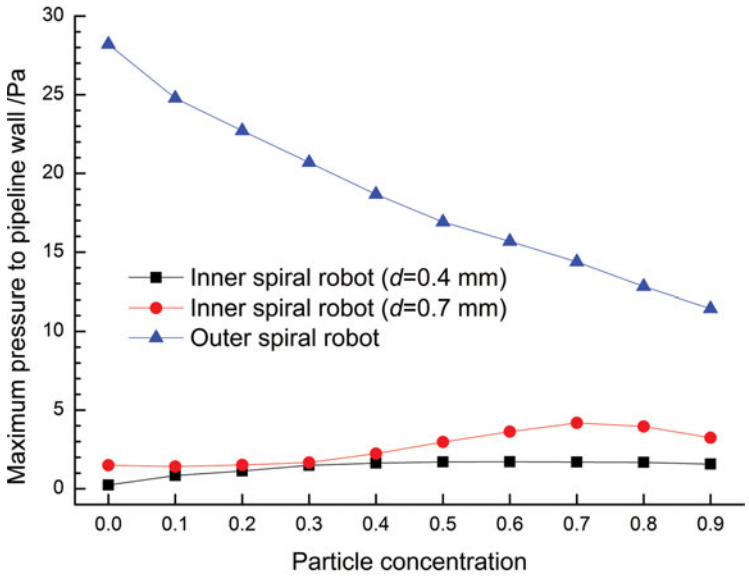

Fig. 13. Relationship between maximum pressure to pipeline wall and concentrations of solid-phase particles.

5.2. Liquid–liquid two-phase fluid environment

5.2.1. Effect of the second-phase liquid concentration. In the calculation, it is assumed that the added second-phase liquid is dispersed homogeneously in the first-phase liquid, and these two liquid-phase fluids remain non-miscible. The second-phase liquid concentration changes from 0.1 to 0.9. Figures 14 to 16 are, respectively, the variation curves of the robotic performance indicators with the second-phase liquid concentrations in the single-phase liquid and the liquid–liquid two-phase fluid. In the figure, the second-phase liquid concentration is 0 that means there is only the first-phase liquid in the pipeline. The second-phase liquid concentration is 1 that means there is only the second-phase liquid in the pipeline. When the second-phase liquid with high viscosity is added to the first-phase liquid, the operational performance indicators of spiral robots increase with the increase of the second-phase liquid concentration. This shows that in the liquid pipeline, the higher the proportion of the liquid with high viscosity is, the better the drive performance of the spiral robot is, while the energy consumption and the pressure to the inner wall of the pipeline are too increased. Similarly, in the liquid–liquid mixed fluid, the performance indicators of the outer spiral robot are much higher than those of the inner spiral robot, and the performance indicators of inner spiral robots with bigger internal diameters are higher than those with smaller internal diameters. In Fig. 14(b), when the second-phase liquid concentration is changed from 0.9 to 1, the axial thrust force of the outer spiral robot is suddenly increased rapidly. This is because when the liquid–liquid two-phase mixed fluid suddenly becomes a high-viscosity single-phase fluid, the degree of turbulence of fluid near the outer surface of the robot is weakened, and the area of the fluid in contact with the outer spiral robot is larger and the thrust force of the fluid on the surfaces of the robot is further accelerated.

5.2.2. Effect of the degree of dispersion of second-phase liquid. In the above numerical analysis, it is assumed that the second-phase liquid is dispersed homogeneously in the first-phase liquid, and the calculation model of multiphase flow is the mixed model. When the second-phase liquid is not dispersed homogeneously in the first-phase liquid, the Euler model is used.

Figures 17 and 18 are the relationships between the axial thrust force of the inner ($d = 4$ mm) and outer spiral capsule robots and the second-phase liquid concentration in the liquid-liquid two-phase fluid environment when the second-phase liquid is or not dispersed homogeneously in the first-phase liquid (i.e. the different mixing state).

It can be seen from the two figures that when the second-phase liquid is dispersed homogeneously in the first-phase liquid, the axial thrust force of the various spiral capsule robots is greater than that when two phase liquids are not homogeneously mixed. This indicates that the proportion of high viscosity liquid and the mixing degree of multiphase liquids are proportional to the driving performance of the spiral capsule robots in a multiphase liquid environment.

https://doi.org/10.1017/S0263574718000954 Published online by Cambridge University Press

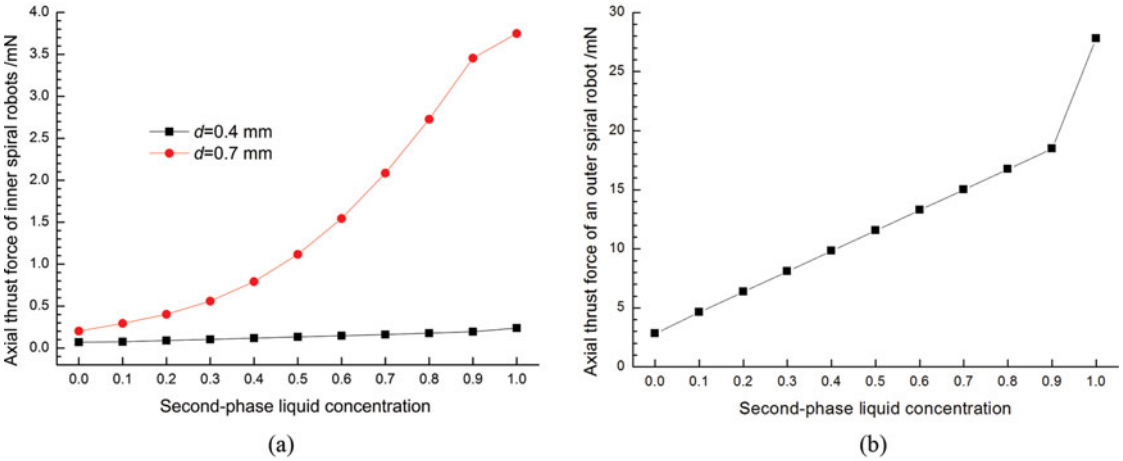

Fig. 14. Relationship between axial thrust force of the robot and second-phase liquid concentration: (a) inner spiral robot and (b) outer spiral robot.

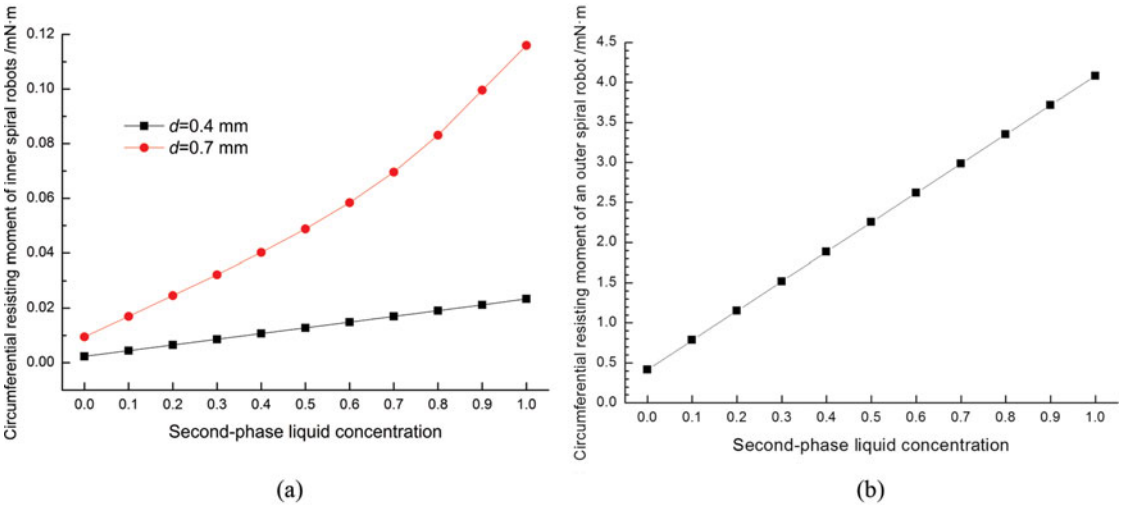

Fig. 15. Relationship between circumferential resisting moment of the robot and second-phase liquid concentration: (a) inner spiral robot and (b) outer spiral robot.

6. Optimum Design of Spiral Capsule Robots in Multiphase Fluid

In fact, an actual environment exists with a determined and special characteristic which is not changeable. We assume that the pipeline is full of liquid–solid two-phase homogeneous mixed fluid, the density of the liquid phase is 1000 kg/m^3 and the dynamic viscosity is 1 Pa·s. The density of the solid phase is 1200 kg/m^3, the dynamic viscosity is 10^{-4} Pa·s, the diameter is 0.1 mm and the concentration in the mixed fluid is 0.1. The optimum design of the spiral capsule robot mainly refers to the structural parameters of the spiral grooves of the robot. The inner spiral robot refers to the inner spiral parameters, and the outer spiral robot refers to outer spiral parameters. The optimization objective of the spiral capsule robot is faster speed, lower energy consumption and no damage, that is, larger axial thrust force, smaller circumferential resisting moment and lower pressure to pipeline wall.

6.1. Structural parameter optimization of the inner spiral capsule robot

Because the inner spiral capsule robot has a smooth surface, the inner spiral structural parameters are shown in Fig. 19 and include: (1) variable a_1 (groove bottom width), (2) variable b_1 (groove top width), (3) dip angle α_1, (4) groove depth h_1, (5) spiral angle Φ_1 and (6) thread number n_1. In Fig. 19, t_1 is inner spiral pitch, d_1 (= 4 mm) is bottom diameter of inner spiral groove and $\Phi_1 = \arctan(n_1 \cdot t_1/(\pi \cdot d_1))$. The outer diameter of the robot is 8 mm, and its axial length is

https://doi.org/10.1017/S0263574718000954 Published online by Cambridge University Press

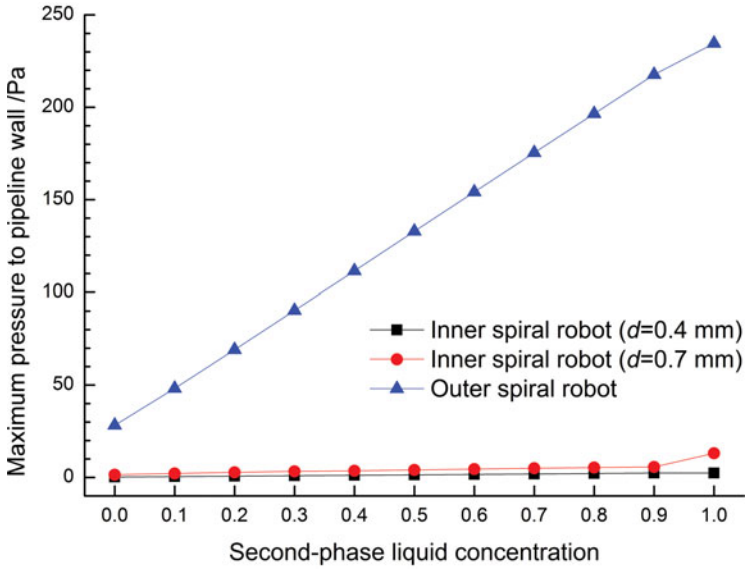

Fig. 16. Relationship between maximum pressure to pipeline wall and second-phase liquid concentration.

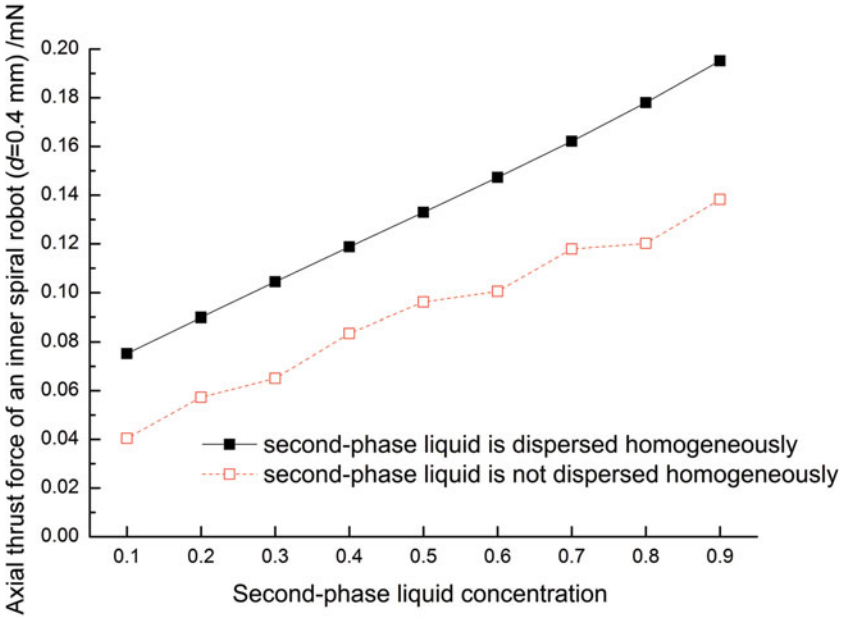

Fig. 17. Relationship between axial thrust force of the inner spiral robot ($d = 0.4$ mm) and second-phase liquid concentration under different mixing states.

15 mm. The pipeline diameter is 12 mm and its length is 75 mm, which are the same as the previous assumptions.

Considering the influences of the six structural parameters on the optimization objective of the robot are not linear and are coupling each other, in order to find the optimal combination of the six parameters, the orthogonal experimental optimization method is introduced.

Six experimental factors are six inner spiral structural parameters. Each factor is given three different typical values to represent three experimental levels, and the experimental indexes are defined as the axial thrust force, circumferential resisting moment and pressure to pipeline wall. If the tests are done, 729 (3^6) tests are needed, and a set of the optimal structural parameters is found. According to the reference,[23] using the orthogonal table $L_{18}(3^6)$ shown in the Table V, we can obtain the optimal solution through only 18 tests.

https://doi.org/10.1017/S0263574718000954 Published online by Cambridge University Press

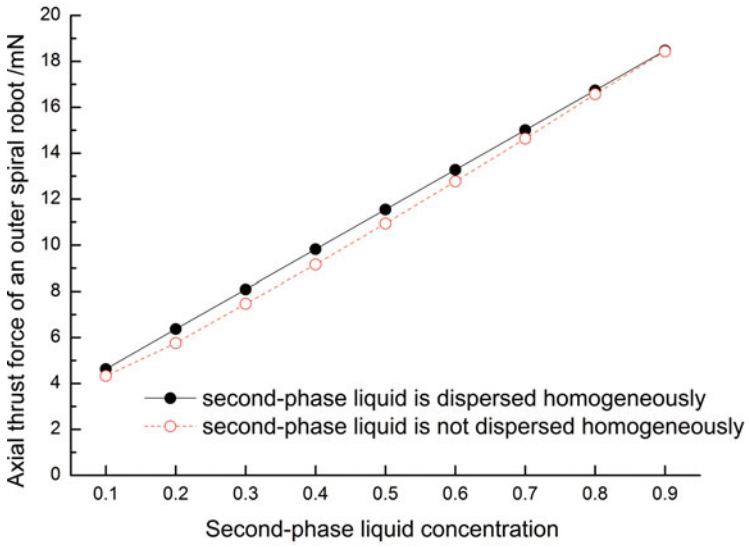

Fig. 18. Relationship between axial thrust force of the outer spiral robot and second-phase liquid concentration under different mixing states.

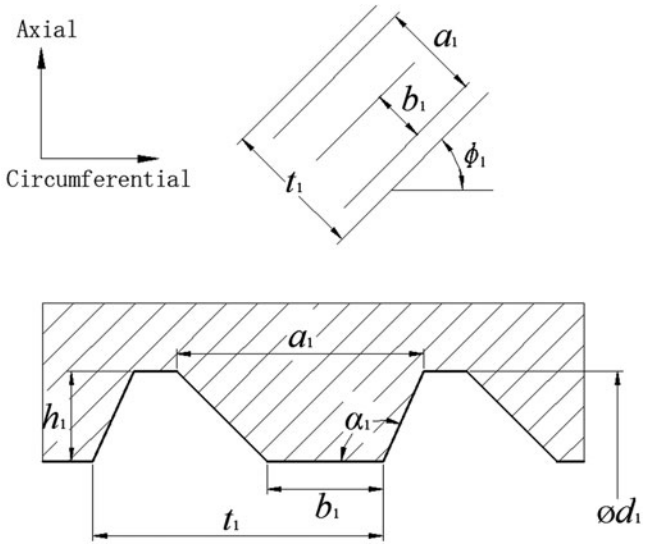

Fig. 19. Inner spiral structural parameters of the inner spiral robot.

The 18 sets of parameters in Table V correspond to 18 different 3D robot system models, and each model is numerically calculated. The results show the optimal inner spiral structural parametrical combination of the robot is as follows: variable a_1 is 0.5 mm, variable b_1 is 0.5 mm, dip angle α_1 is 90°, groove depth h_1 is 0.6 mm, spiral angle Φ_1 is 40° and thread number n_1 is 8. The axial thrust force of the robot is 0.193 mN, the circumferential resisting moment of the robot is 0.0015 mN·m and the maximum pressure to pipeline wall is 3.13 Pa, that is, the largest axial thrust force, smaller circumferential resisting moment and appropriate pressure to pipeline wall.

In order to let these parameters (a_1, b_1, and h_1) be dimensionless, we define parameters β_{11} (a_1/t_1), β_{12} (b_1/t_1) and γ_1 (h_1/d_1). So the optimum design of the inner spiral capsule robot is as follows: parameter β_{11} is 0.38, parameter β_{12} is 0.38, dip angle α_1 is 90°, parameter γ_1 is 0.15, spiral angle Φ_1 is 40° and thread number n_1 is 8.

6.2. Structural parameter optimization of the outer spiral capsule robot

The outer spiral structural parameters of the outer spiral capsule robot are shown in Fig. 20 and include: (1) variable a_2 (groove top width), (2) variable b_2 (groove bottom width), (3) dip angle α_2,

https://doi.org/10.1017/S0263574718000954 Published online by Cambridge University Press

Table V. Orthogonal experiment of inner spiral structural parameters of the inner spiral robot.

No.	a_1 (mm)	b_1 (mm)	α_1 (°)	h_1 (mm)	Φ_1 (°)	n_1	Axial thrust force (mN)	Circumferential resisting moment (mN·m)	Pressure to pipeline wall (Pa)
1	0.5	0.75	70	0.2	40	6	0.085	0.0016	0.76
2	0.5	0.75	90	1	45	10	0.027	0.0020	3.08
3	0.75	0.5	90	0.2	50	8	0.009	0.0026	3.00
4	0.75	1	110	0.6	40	6	0.041	0.0024	3.04
5	1	0.5	110	0.6	45	10	0.029	0.0021	3.05
6	1	1	70	1	50	8	0.130	0.0020	3.16
7	0.5	0.5	110	1	50	6	0.055	0.0015	3.13
8	0.5	1	110	0.2	45	8	0.144	0.0019	3.07
9	0.75	0.5	70	1	45	10	0.122	0.0020	3.00
10	0.75	0.75	70	0.6	40	8	0.028	0.0024	3.02
11	1	0.75	90	0.6	50	6	0.095	0.0017	3.23
12	1	1	90	0.2	40	10	0.039	0.0021	3.04
13	**0.5**	**0.5**	**90**	**0.6**	**40**	**8**	**0.193**	**0.0015**	**3.13**
14	0.5	1	70	0.6	50	10	0.054	0.0017	3.04
15	0.75	0.75	110	0.2	50	10	0.018	0.0020	2.98
16	0.75	1	90	1	45	6	0.059	0.0017	3.03
17	1	0.5	70	0.2	45	6	0.088	0.0016	3.12
18	1	0.75	110	1	40	8	0.065	0.0016	3.13

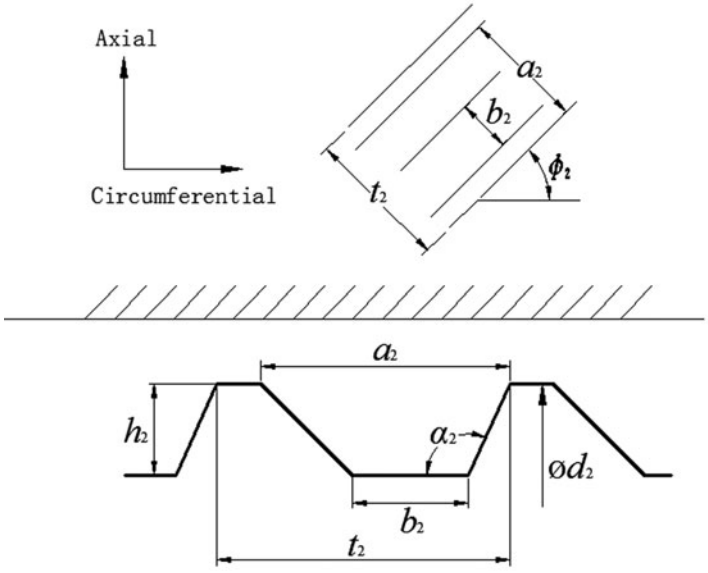

Fig. 20. Outer spiral structural parameters of the outer spiral robot.

(4) groove depth h_2, (5) spiral angle Φ_2 and (6) thread number n_2. In Fig. 20, t_2 is outer spiral pitch, d_2 is the outer diameter of outer spiral robot and $\Phi_2 = \arctan(n_2 \cdot t_2/(\pi \cdot d_2))$. The outer diameter ($d_2$) of the robot is 8 mm, and its axial length is 15 mm. The pipeline diameter is 12 mm and its length is 75 mm, which are the same as the previous assumptions.

Similarly, six experimental factors are six outer spiral structural parameters. Each factor is given five different typical values to represent five experimental levels, and the experimental indexes are defined as the axial thrust force, circumferential resisting moment and pressure to pipeline wall. If the tests are done, 15,625 (5^6) tests are needed, and a set of the optimal structural parameters is found. According to the reference,[23] using the orthogonal table $L_{20}(5^6)$ shown in the Table VI, we can obtain the optimal solution through only 20 tests.

https://doi.org/10.1017/S0263574718000954 Published online by Cambridge University Press

Table VI. Orthogonal experiment of outer spiral structural parameters of the outer spiral robot.

No.	a_a (mm)	b_2 (mm)	α_2 (°)	h_2 (mm)	Φ_2 (°)	n_2	Axial thrust force (mN)	Circumferential resisting moment (mN·m)	Pressure to pipeline wall (Pa)
1	0.25	0.5	70	1	50	7	0.57	0.418	31.68
2	0.5	0.5	110	0.8	35	9	0.83	0.405	39.42
3	0.75	1.25	50	0.6	40	10	1.86	0.397	37.19
4	1.25	0.75	90	1.2	40	6	2.11	0.396	37.98
5	0.5	1	110	0.4	45	8	0.32	0.395	50.55
6	0.75	0.75	30	0.4	30	6	1.16	0.404	43.73
7	1	0.25	50	1	30	8	1.99	0.370	39.27
8	1	1.25	70	1.2	50	9	1.20	0.399	47.52
9	0.25	0.25	70	0.6	35	6	0.12	0.412	36.55
10	0.5	1	30	1.2	35	10	0.79	0.397	33.67
11	1.25	0.25	90	0.4	40	9	0.83	0.373	34.31
12	1.25	1.25	30	0.8	45	7	1.47	0.401	47.28
13	0.25	1.25	90	1	30	8	0.24	0.401	42.87
14	0.75	0.25	110	1	45	10	0.88	0.410	26.42
15	1	0.5	30	0.6	50	8	0.49	0.420	30.45
16	1	1	110	0.6	35	7	2.57	0.399	38.54
17	0.25	0.75	50	0.4	45	9	0.14	0.413	53.10
18	0.5	0.5	50	1.2	40	7	0.29	0.408	37.52
19	0.75	1	90	0.8	50	6	0.40	0.418	35.18
20	**1.25**	**0.75**	**70**	**0.8**	**30**	**10**	**4.04**	**0.383**	**34.98**

The 20 sets of parameters in Table V correspond to 20 different 3D robot system models, and each model is numerically calculated. The results show the optimal outer spiral structural parametrical combination of the robot is as follows: variable a_2 is 1.25 mm, variable b_2 is 0.75 mm, dip angle α_2 is 70°, groove depth h_1 is 0.8 mm, spiral angle Φ_2 is 45°, and thread number n_2 is 10. The axial thrust force of the robot is 4.04 mN, the circumferential resisting moment of the robot is 0.383 mN·m and the maximum pressure to pipeline wall is 34.98 Pa, that is, the largest axial thrust force, smaller circumferential resisting moment and lower pressure to pipeline wall.

In order to let these parameters (a_2, b_2 and h_2) be dimensionless, we define parameters β_{21} (a_2/t_2), β_{22} (b_2/t_2) and γ_2 (h_2/d_2). So the optimum design of the outer spiral capsule robot is as follows: parameter β_{21} is 0.5, parameter β_{22} is 0.3, dip angle α_2 is 70°, parameter γ_2 is 0.1, spiral angle Φ_2 is 30° and thread number n_2 is 10.

7. Experimental Verification

In order to verify the effect of solid particles and another liquid of high viscosity on the performance of spiral robots in a pipeline containing liquid, the designed and manufactured prototype of the inner spiral robot[18] is used to carry out some experiments, as shown in Fig. 21. In the experiment, the working pipeline is a transparent plexiglass tube, and the first-phase liquid is the 201 methyl silicone oil with the dynamic viscosity of 1 Pa·s, as shown in Fig. 22. Solid particles are crystal muds, and their diameters range from 0.2 to 0.8 mm, as shown in Fig. 23. The added second-phase liquid is also the 201 methyl silicone oil, and its dynamic viscosity ranges from 2 Pa·s to 10 Pa·s.

Figure 24 shows the variation curve of the measured moving average speed of the inner spiral robot prototype with the change of the diameters of solid-phase particles when the concentration of solid-phase particles is 0.1. In the liquid–solid two-phase fluid, as the diameter of the solid-phase particles is increased, the moving average speed of the robot decreases from 1.52 mm/s to 1.13 mm/s.

Figure 25 shows the variation curve of the measured moving average speed of the inner spiral robot prototype with the change of the concentrations of solid-phase particles when the diameter of solid-phase particles is 0.2 mm. The concentration of solid-phase particles of 0 indicates a single-phase liquid flow environment in which solid-phase particles are not added. In the single-phase liquid, the

https://doi.org/10.1017/S0263574718000954 Published online by Cambridge University Press

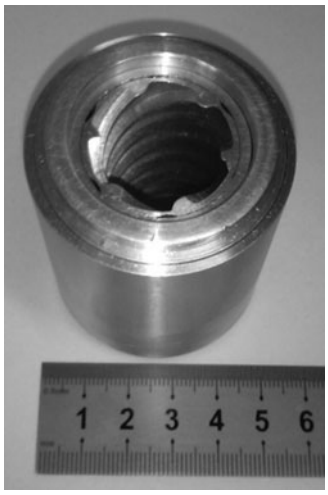

Fig. 21. Prototype of inner spiral robot.

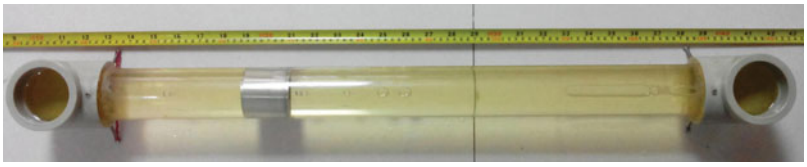

Fig. 22. Inner spiral robot in 201 methyl silicone oil.

Fig. 23. Solid particles.

moving average speed of the robot is 2.0 mm/s. When the number of added solid particles with a fixed diameter is increased, the moving average speed of the robot gradually decreases.

When the second-phase liquid is dispersed homogeneously in the pipeline containing the first-phase liquid, the moving speed of the robot increases with the increase of the second-phase liquid concentration, and its value can reach 2.9 m/s. Therefore, the experimental results show that the existence of solid particles reduces the drive performance of the inner spiral capsule robot in the pipeline containing liquid, and the addition of another liquid of high viscosity in the pipeline containing one liquid improves the operational performance of the inner spiral capsule robot.

8. Conclusions and Future Works

The present study of spiral capsule robots is aimed at a pipeline filled with single-phase liquid. In this paper, the CFD method is used to calculate the relationship between operational performance indicators (i.e. axial thrust force, circumferential resisting moment and maximum pressure to pipeline wall) of inner spiral capsule robots with different internal diameters and outer spiral capsule robots and solid particle diameter, solid particle concentration and second-phase liquid concentration in the liquid–solid or liquid–liquid mixed two-phase fluid, and the verification experiments are completed.

In the liquid–solid two-phase fluid, when the particle size or concentration is increased, the axial thrust force and circumferential resisting moment of the spiral capsule robots decrease, but the

https://doi.org/10.1017/S0263574718000954 Published online by Cambridge University Press

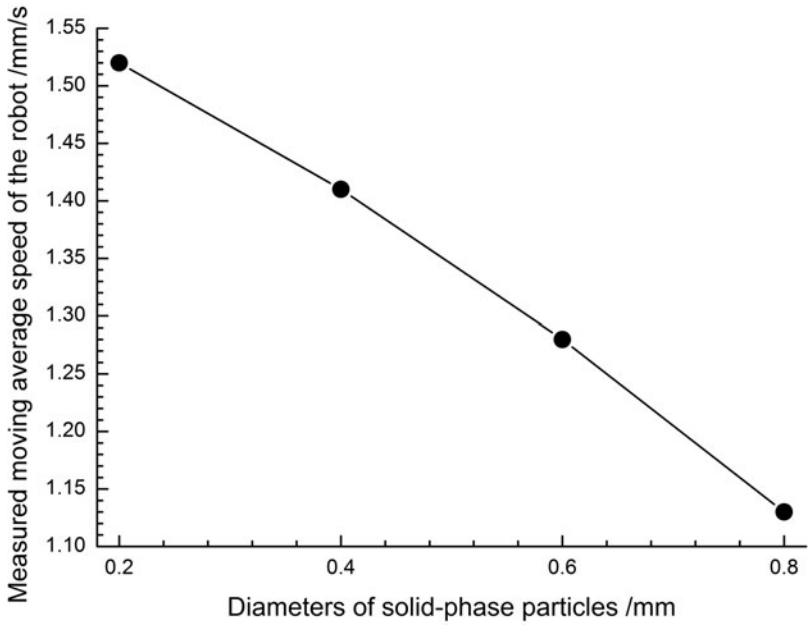

Fig. 24. Relationship between average moving velocity of the robot measured by the test and diameters of solid-phase particles.

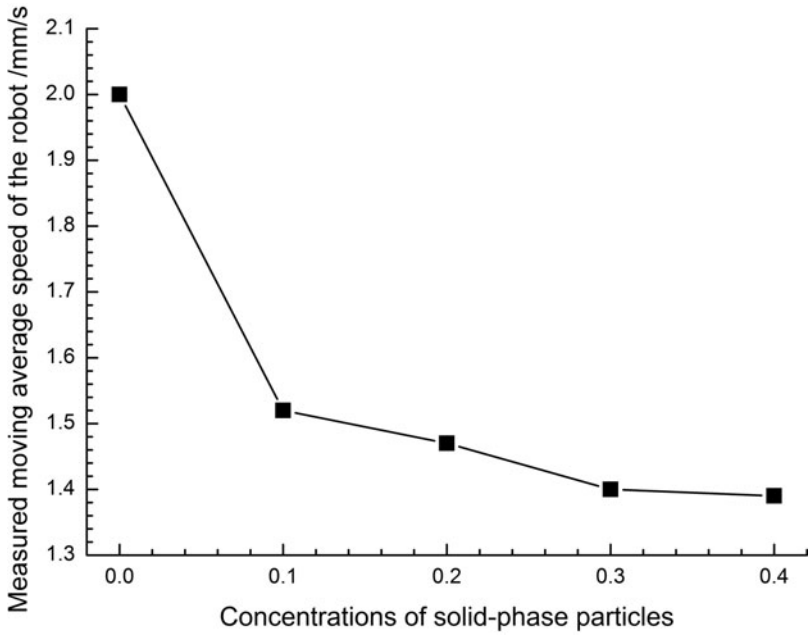

Fig. 25. Relationship between moving average velocity of the robot measured by the test and concentrations of solid-phase particles.

maximum pressure to pipeline wall indefinitely changes. The effect of particle sizes on the operational performance of spiral capsule robots is less than particle concentrations on that. In the liquid–solid mixed fluid of the same particle size and concentration, the performance indicators of the outer spiral robot are much higher than those of the inner spiral robot, and the performance indicators of inner spiral robots with bigger internal diameters are higher than those with smaller internal diameters. The addition of solid particles in the pipeline containing liquid will reduce the drive performance of the spiral capsule robot.

https://doi.org/10.1017/S0263574718000954 Published online by Cambridge University Press

When the second-phase liquid with high viscosity is added to the pipeline containing the first-phase liquid, the operational performance indicators of spiral robots increase with the increase of the second-phase liquid concentration. In the liquid–liquid mixed fluid, the performance indicators of the outer spiral robot are much higher than those of the inner spiral robot, and the performance indicators of inner spiral robots with bigger internal diameters are higher than those with smaller internal diameters. To improve the drive performance of the spiral capsule robot, another high-viscosity liquid can be added to the pipeline containing one liquid.

By the orthogonal experimental optimization method, the optimum design of spiral capsule robots is obtained in the liquid–solid mixed fluid. When the pipeline is full of liquid–solid two-phase homogeneous mixed fluid, the density of the liquid phase is 1000 kg/m^3, and the dynamic viscosity is 1 Pa·s. The density of the solid phase is 1200 kg/m^3, the dynamic viscosity is 10^{-4} Pa·s, the diameter is 0.1 mm and the concentration in the mixed fluid is 0.1. The outer diameter of the robot is 8 mm, its axial length is 15 mm, the pipeline diameter is 12 mm and its length is 75 mm. The optimum design of the inner spiral capsule robot is as follows: parameter β_{11} is 0.38, parameter β_{12} is 0.38, dip angle α_1 is 90°, parameter γ_1 is 0.15, spiral angle Φ_1 is 40° and thread number n_1 is 8. The optimum design of the inner spiral capsule robot is as follows: parameter β_{21} is 0.5, parameter β_{22} is 0.3, dip angle α_2 is 70°, parameter γ_2 is 0.1, spiral angle Φ_2 is 30° and thread number n_2 is 10.

Due to changes of the intestinal pressure, it may produce gas, and even there exists cavitation phenomenon. Therefore, when the pipeline is filled with liquid—solid–gas three-phase fluid, the operational performance and optimum structure of the spiral capsule robot are the next content to study. Furthermore, the size of the spiral capsule robot prototype will be miniaturized so that it can be tested in human or animal intestines.

Acknowledgments

This work was supported in part by National Natural Science Foundation of China (Grants No. 51875051 and 51575256) and in part by Scientific Research Fund of the Hunan Provincial Education Department (Grants No. 16A019 and 14B020).

References

1. Z. Liao, Z. S. Li and Z. D. Jin, *Mapping of Gastrointestinal Remote Capsule Endoscopy* (Tsinghua University Press, Beijing, 2015).
2. G. D. Meron, "The development of the swallowable video-capsule (M2A)," *Gastrointestinal Endoscopy* **52**(6), 812–819 (2000).
3. R. F. Sayaka, System Lab. [EB/OL]. Available at: http://www.rfsystemlab.com/en/sayaka/ (2014).
4. H. J. Park, H. W. Nam, B. S. Song *et al.*, "Design of Bi-directional and Multi-channel Miniaturized Telemetry Module for Wireless Endoscopy," *Proceedings of the 2nd Annual International IEEE-EMB Special Topic Conference on Microtechnologies in Medicine & Biology*, Madison, USA (2002) pp. 273–276.
5. S. Maqbool, H. P. Parkman and F. K. Friedenberg, "Wireless capsule motility: Comparison of the Smartpill GI monitoring with scintigraphy for measuring whole gut transit," *Digestive Diseases Sci.* **54**(10), 2167–2174 (2009).
6. A. A. Calderón, J. C. Ugalde, J. C. Zagal *et al.*, "Design, Fabrication and Control of a Multi-Material-Multi-Actuator Soft Robot Inspired by Burrowing Worms," *Proceedings of the IEEE International Conference on Robotics and Biomimetics*, Qingdao, China (2016) pp. 31–38.
7. J. Z. Ge, A. A. Calderón and N. O. Pérez-Arancibia, "An earthworm-inspired soft crawling robot controlled by friction," *Proceedings of the IEEE International Conference on Robotics and Biomimetics*, Macau, China (2017) pp. 834–841.
8. B. Kim, M. G. Lee, Y. P. Lee *et al.*, "An earthworm-like micro robot using shape memory alloy actuator," *Sensors Actuators A Phys.* **125**(2): 429–437 (2006).
9. C. Zhang, G. Su, R. J. Tan, and H. Y. Li "Experimental Investigation of the Intestine's Friction Characteristic based on "Internal Force-Static Friction" Capsubot," *Proceedings of the IASTED International Conference Biomedical Engineering*, Innsbruck, Austria (2011) pp. 16–18.
10. S. H. Woo, T. W. Kim, Z. Mohy-Ud-Din, I. Y. Park and J. H. Cho "Small intestinal model for electrically propelled capsule endoscopy," *Biomed. Eng. Online* **10**(1), 1–20 (2011).
11. S. He, G. Z. Yan,Q. Ke *et al.*, "A wirelessly powered expanding-extending robotic capsule endoscope for human intestine," *Int. J. Precision Eng. Manuf.* **16**(6), 1075–1084 (2015).
12. M. Sendoh and K. Ishiyama, "Fabrication of magnetic actuator for use in a capsule endoscope," *IEEE Trans. Magn.* **39**(5), 3232–3234 (2003).

13. Y. S. Zhang, S. Y. Jiang, X. W. Zhang *et al.* "A variable-diameter capsule robot based on multiple wedge effects," *IEEE/ASME Trans. Mechatronics* **16**(2), 241–254 (2011).
14. H. Zhou, G. Alici, T. D. Than *et al.*, "Modeling and experimental characterization of propulsion of a spiral-type microrobot for medical use in gastrointestinal tract," *IEEE Trans. Biomed. Eng.* **60**(6), 1751–1759 (2013).
15. N. Liang, J. Guo, S. Guo *et al.*, "Performance Evaluation of the Wireless Micro Robot in the Fluid," *Proceedings of the IEEE International Conference on Mechatronics and Automation*, Beijing, China (2015) pp. 958–963.
16. J. Guo, S. Guo, X. Wei *et al.*, "A novel tele-operation controller for wireless microrobots in-pipe with hybrid motion," *Robot. Autonomous Syst.* **76**(C), 68–79 (2016).
17. L. Liang, B. Chen, Y. Tang *et al.*, "Research on a novel inner and outer spiral micro in-pipe robot," *J. Adv. Mech. Design Syst. Manuf.* **8**(6), 1–14 (2014).
18. L. Liang, H. Peng, B. Chen *et al.*, "Performance analysis and parameter optimization of an inner spiral in-pipe robot," *Robotica* **34**(2), 361–382 (2016).
19. L. Liang, R. Hu, B. Chen *et al.*, "Scaling effects in spiral capsule robots," *Proc. Institution Mech. Eng. H J. Eng. Med.* **231**(4), 307–314 (2017).
20. D. H. Zhou, J. S. Li, N. Li *et al.*, "Study on viscosity property of gastrointestinal," *J. Biomed. Eng.* **21**(1), 72–73 (2004).
21. Z. Wang, M. Zhou, D. M. Su *et al.*, "Experimental study concerning the effects of profile morphology of intestine on the frictional characteristics," *Tribology* **34**(2), 193–197 (2014).
22. F. Jiang and P. Huang, *Fluent Advanced Application and Case Analysis* (Tsinghua University Press, Beijing, 2008).
23. K. Fang and C. Ma, *Orthogonal and Uniform Experimental Design* (Science Press, Beijing, 2001).